



# Experimental and computational approach to human brain modelling – aHEAD

Mariusz Ptak<sup>1</sup> · Mateusz Dymek<sup>1</sup> · Marek Sawicki<sup>1</sup> · Fábio A. O. Fernandes<sup>2</sup> · Maciej Wnuk<sup>1</sup> · Johannes Wilhelm<sup>3</sup> · Monika Ratajczak<sup>4</sup> · Daria Witkowska<sup>5</sup> · Artur Kwiatkowski<sup>6</sup> · Błażej Poźniak<sup>7</sup> · Konrad Kubicki<sup>8</sup> · Marta Tikhomirov<sup>9</sup> · Adam Druszcz<sup>6</sup> · Leszek Chybowski<sup>10</sup>

Received: 4 April 2023 / Revised: 19 July 2023 / Accepted: 20 July 2023  
© The Author(s) 2023

## Abstract

The human head is a highly complex structure, with a combination of hard and soft tissues and a variety of materials and interactions. Many researchers have used computational approaches to model the head, and several human finite element head models can be found in the literature. However, most of them are not geometrically accurate – for instance, the brain is simplified to a smooth spherical volume, which poses some concerns regarding boundary conditions and geometrical accuracy. Therefore, an advanced head model of a 28-year-old, designated as aHEAD 28 yo (aHEAD: advanced Head models for safety Enhancement And medical Development), has been developed. The model consists entirely of hexahedral elements for 3D structures of the head such as the cerebellum, skull and cerebrum, with detailed geometry of the gyri and sulci. Additionally, it is one of the first human head approaches published in the literature that includes cerebrospinal fluid simulated by Smoothed Particle Hydrodynamics (SPH) and a detailed model of pressurized bridging veins. To support the model's credibility, this study is focused on physical material testing. A novel comprehensive experimental-computational approach is presented, which involves the brain tissue's response to induced vibrations. The experiment successfully aimed to validate the material models used in the numerical analysis. Additionally, the authors present a kinematical model validation based on the Hardy experimental cadaver test. The developed model, along with its verification, aims to establish a further benchmark in finite element head modelling and can potentially provide new insights into injury mechanisms.

**Keywords** Finite element head model · Numerical model · Material modelling · Induced vibrations · Head injury · Injury criteria · Brain · Numerical simulation · Head kinematics

## 1 Introduction

Traumatic brain injury (TBI) represents a significant portion of the global injury burden [1]. Annually, around 27 million TBI cases are reported worldwide [2]. Head trauma may occur in a great variety of activities, from sports to road accidents. The outcome of head impacts in some of these activities can be very severe, resulting in long-term injuries and permanent disability or death in the most extreme cases. Therefore, TBI burdens healthcare systems and economies through lost productivity and high healthcare costs [3].

TBI is caused primarily by falls and road injuries [4]. Over time, the increase in TBI incidence may continue given increased population density, population ageing, and expanded use of motor vehicles, motorcycles, and bicycles

[2]. In addition to the mobility patterns, the number of individuals involved in sports is rapidly increasing, supported by the health benefits, and starting at very young ages. Therefore, it is believed that TBI will continue to be a significant burden in the future.

Finite element (FE) models of the human head have been developed to study head injury mechanisms, to reconstruct trauma events or simulate potential ones, from forensic cases [5] and crash tests [6] to head impacts in motorsports [7, 8], contact sports [9] and military [10]. After validation, such a model is a valuable tool for predicting head injury on a virtual test basis and optimizing headgear [11], vehicle structures [12] or surfaces typically involved in head impacts [13, 14].

In the literature, there are several head models utilizing the finite element method (FEM), some of which have been updated over the years by including more structures,

Extended author information available on the last page of the article

improving geometrical accuracy and FE mesh, using adequate non-linear constitutive models and FE formulation, or simply verifying the model robustness and validation by increasing the number of simulated case studies and benchmarking [15]. Examples can be found in the following manuscripts published by Dixit [16], Fernandes [17], Giudice [18]; Madhukar [19] and Wang et al. [20]. Although several models can be found in the literature, most are not geometrically accurate. For instance, the brain is a smooth spherical volume in most models. There were recent concerns regarding boundary conditions and geometrical accuracy. Still, the primary approach involves employing linear tetrahedral FEs, which tend to be a numerical burden since most human tissues are incompressible, resulting in numerical locking problems. Second-order tetrahedral elements are a solution, but at the cost of higher computational time and possible negative volume errors [21].

Most advanced FE head models already have dual-matter brains e.g., published by Zhao [22], Zhou [23], or Wilhelm et al. [24]. A few have recently considered modelling sulci and gyri cerebral structures [25–27]. The studies concluded that these structures are relevant to the overall behaviour of the brain, especially for the prediction of intracranial relative displacement and injuries such as cerebral contusions. Moreover, Weickenmeier et al. [26] considered white and grey matters and gyri and sulci structures.

The relative motion between the skull and brain may cause cerebral contusion or bridging vein failure leading to subdural haematoma. Cerebrospinal fluid (CSF) is essential to represent brain-skull relative displacement and intracranial pressure. Recently, some research groups have focused on fluid–structure interaction [28–30]. The CSF is usually modelled as a solid volume with a low shear modulus and a high Poisson's ratio to make it easily deformable and incompressible. Jin et al. [28] modelled skull-CSF-brain interaction based on the arbitrary Lagrangian–Eulerian (ALE) and overlapping mesh methods. It was found that the skull-brain relative displacement and brain injury prediction may benefit from implementing the ALE method. More recently, other researchers have adopted the ALE formulation to model CSF [30]. Another approach recently implemented to improve the simulation of intracranial fluid–solid interactions is based on using the smoothed-particle hydrodynamics (SPH) method to model the CSF with particles – e.g. presented by Toma [31] and Ptak et al. [24].

FE head modelling is currently used to understand several aspects of head trauma. If properly validated, these models can predict the occurrence of injuries and optimize safety gear. Nevertheless, they must be developed taking into account essential factors such as age, sex and anthropometry to represent as broad a population group as possible if aiming to be general studies [32, 33].

This study presents an advanced FE head model of a young adult male. A particular FE meshing strategy was adopted, making it possible to model complex geometrical structures such as the brain with high geometrical accuracy using a good quality FE mesh employing first-order hexahedral elements.

Additionally, white and grey matter detailed segmentation and experimental tests on porcine brain matter were carried out to validate the constitutive strategy adopted for this brain model. As highlighted in [34], to provide mechanical properties for such models, there is a need to characterize mixed grey/white matter samples. Likewise, the meshless SPH method was employed to model the fluid–structure interaction between the CSF and the other intracranial components, filling the subarachnoid space with particles. The cerebral vasculature, from high-calibre vessels such as the superior sagittal sinus (SSS) and transverse sinus to the thinner bridging veins (BVs), including the veins of Labbé and Trolard (or inferior and superior anastomotic veins, respectively), was also modelled. The latter ones have been so far often omitted, even in FE head models with detailed vasculature systems and high levels of accuracy [35, 36]. After finalizing the modelling stage, the model was employed to simulate one of the benchmark tests, the relative displacement between brain and skull, from Hardy experiments [37, 38]. As a result, an advanced 28-year-old model, named aHEAD 28yo, was developed, which advances the state-of-the-art in predicting the effects of brain trauma.

## 2 Materials and methods

### 2.1 Experimental phase

In the first phase of the experiment, brain samples were tested using a shaking machine (specimen shaker) that had been developed in-house. Fresh porcine brains were obtained from a commercial slaughterhouse, and their use did not require consent from any ethical or regulatory bodies. The experiment was carried out in stable conditions to minimize the influence of external factors on the experiment. The shaking machine was created to minimize the influence of gravity on the measurements – hence it was built horizontally. The inductor – MTS Systems Model 2100E11 – was connected to the base frame and rail, producing vibrations. The test bench for vibration examination was designed as a guide rail and carriage with an attached sample holder. Vibrations were generated by the inductor attached to the frame. Inductor output vibrations were transferred by a rod to the test bench and sample holder Fig. 1.

The imposing signal was an audio file sent to a QSC RMX2450 amplifier that was directly connected to the shaker. For imposing signal generation, a Python script was

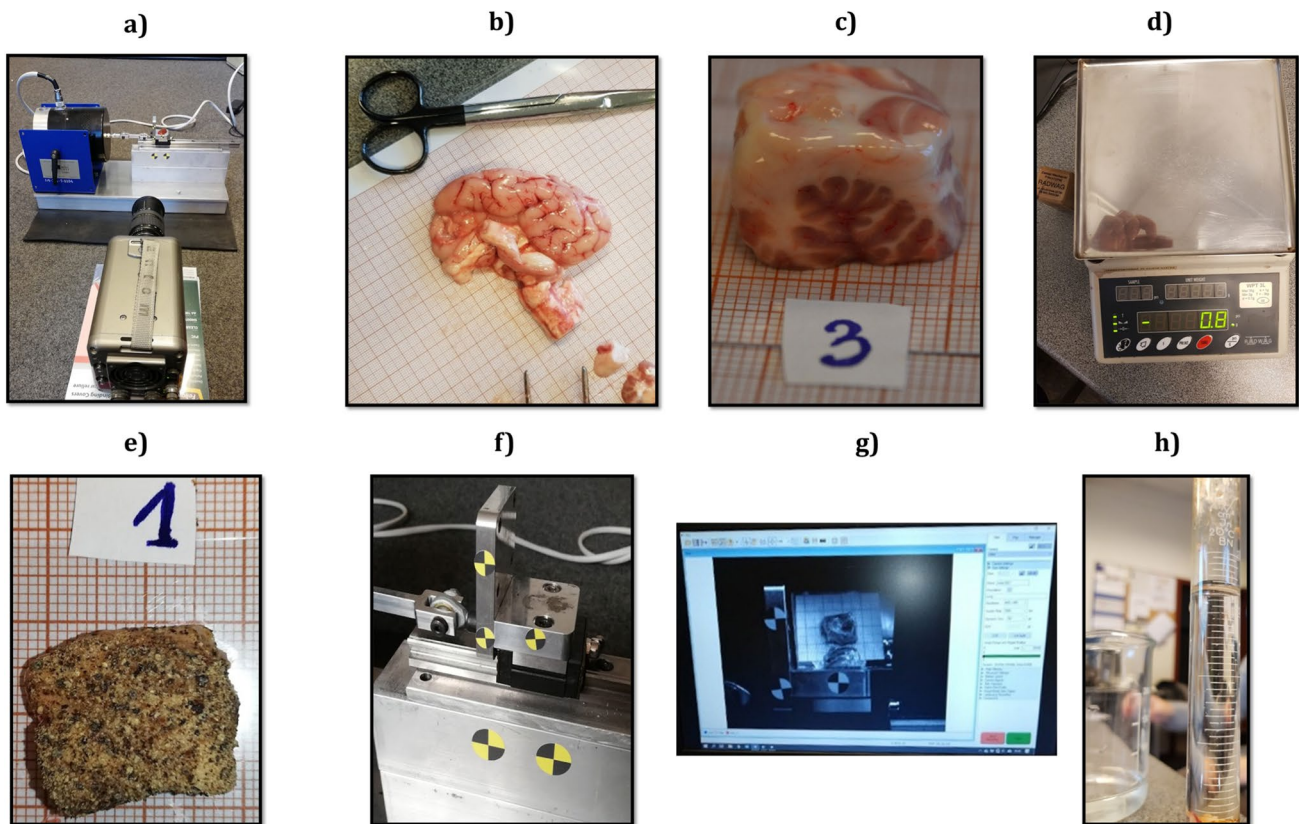


**Fig. 1** Stages undertaken in the physical material experiments: **a** Preparation of the work stand **b** Cutting brain into samples **c** Numbering the samples **d** Weighing each brain sample **e** Preparing the sam-

ples **f** In situ shaking machine experiment **g** Experimental measurements **h** Measuring sample's volume

written, which created a wav file with variable frequency and sinusoidal amplitude. The script allowed the instrument to impose a sine sweep test of constant acceleration, which was used to find the resonance frequency of the system (see the Python script in our repository <https://doi.org/10.5281/zenodo.7503989>). The generated waveform was created according to the following formula:

Logarithmic frequency change with respect to time:

$$f(t) = f_0 \cdot \beta^t$$

$$\beta = \left( \frac{f_1}{f_0} \right)^{\frac{1}{T}} \quad (1)$$

Imposed amplitude proportional to velocity (inducer controlled by voltage):

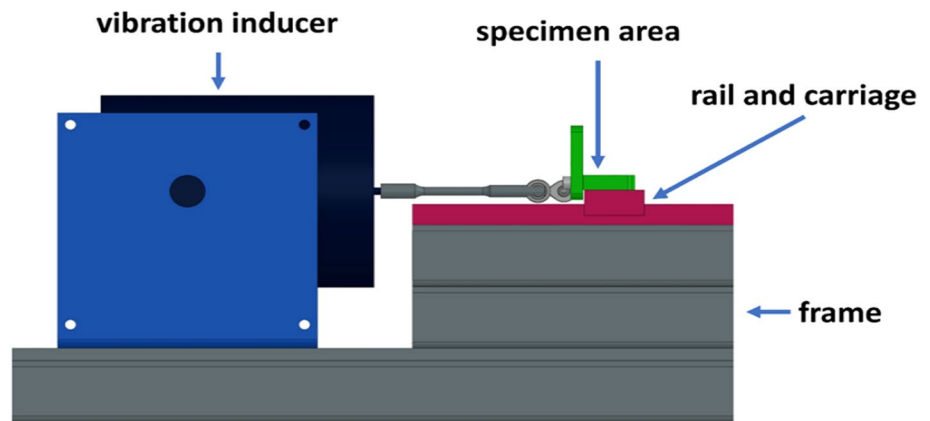
$$v = \frac{a}{2 \cdot \pi \cdot f} \quad (2)$$

where: where  $f$  is frequency,  $t$  is time,  $f_0$  is starting frequency,  $f_1$  is the frequency at the end of the test,  $T$  is the time of the test,  $v$  is the velocity and  $a$  is the requested acceleration. The test stand is presented in Fig. 2.

All experiments were completed within 12h from the animal's death, and the brain tissue was refrigerated (4 °C) during the time preceding the tests. Shortly before the experiments, the tissue was cut into small samples, approximately 20 × 30 mm, and allowed to reach room temperature. It was important to identify from which part of the brain the sample was extracted. During the experiment, samples were taken from four parts of the brain: the medulla, cerebellum, cerebral hemisphere and brain nuclei. Each sample of the brain was put on a scale to measure its mass. After this stage, it was important to perform the experiment as quickly as possible to prevent the sample drying. After mechanical testing, the volume of the sample was measured. A summary of all tested samples is displayed in the repository files 'Experiment sample: <https://doi.org/10.5281/zenodo.7503989> as well as in the appendix Table 3.

A single high-speed Phantom camera setup at 1,000 fps was used with a 45° mirror, allowing the authors to record two perpendicular sides of a specimen in one picture. This invention was applied successfully, and it is recommended by the authors. Due to the vibration movement of the excitation, a high-speed camera was used to record several

**Fig. 2** Designed specimen shaker for the material tests



frames of the test bench with specimens in half of the cycle – between the two extreme positions.

Results that were collected from the experiment are the relative-to-base displacements of the characteristic points on the specimen (Fig. 3). Point 1 is in the right-upper corner, point 2 in the middle of the sample and point 3 in the left-upper corner. The sample video footage of the test is presented here: [https://youtu.be/Ox2klvF1\\_1c](https://youtu.be/Ox2klvF1_1c).

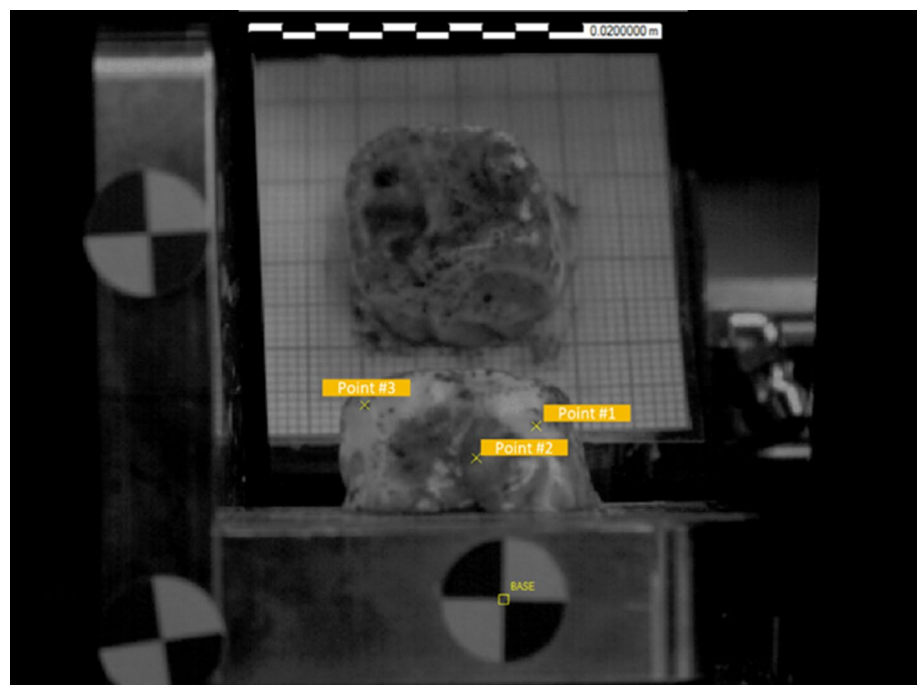
## 2.2 FEM model validation phase

The second phase of this research was the numerical material model validation based on the sample behaviour with induced vibration. Hence, we recreated the samples using computer-aided design (CAD) software and conducted the

simulations with LS-DYNA software [39]. The simulation was conducted to mimic the real support and mounting of the brain specimen, so the nodes on the bottom surface were fixed in all degrees of freedom besides Y translation (Fig. 4–left). For these nodes, the extension in the Y direction was given by the displacement amplitude, which was obtained from the physical experiment (Fig. 4–right). The amplitude was equal to the amplitude of the base point, which was tracked during the experiment via the high-speed camera tracking software, TEMA. The highlighted sets of nodes correspond to the tracked points in Fig. 3. The displacement plotted in \\* MERGEFORMAT Fig. 4 is a node averaged value for each point.

The most suitable material model used for the experiment – among the many tested by the researchers – turned

**Fig. 3** A sample on the shaker with marked tracking points and a reference base point





out to be the material model presented in Total Human Model for Safety (THUMS) [40], the parameters of which are shown in Table 1. The validation procedure was based on the displacement response to the induced vibrations. All the tested material configurations, i.e. used in THUMS, GHBM (Global Human Body Models Consortium) as well as Mooney-Rivlin and Ogden are available

in the online repository (<https://doi.org/10.5281/zenodo.7503989>).

The material model employed enabled the authors to obtain a good correlation in terms of the displacement peak values, i.e. the amplitude and wave period overlapping – especially after 80 ms the physical specimen was stabilized (Fig. 5). We could observe that the amplitude of the points

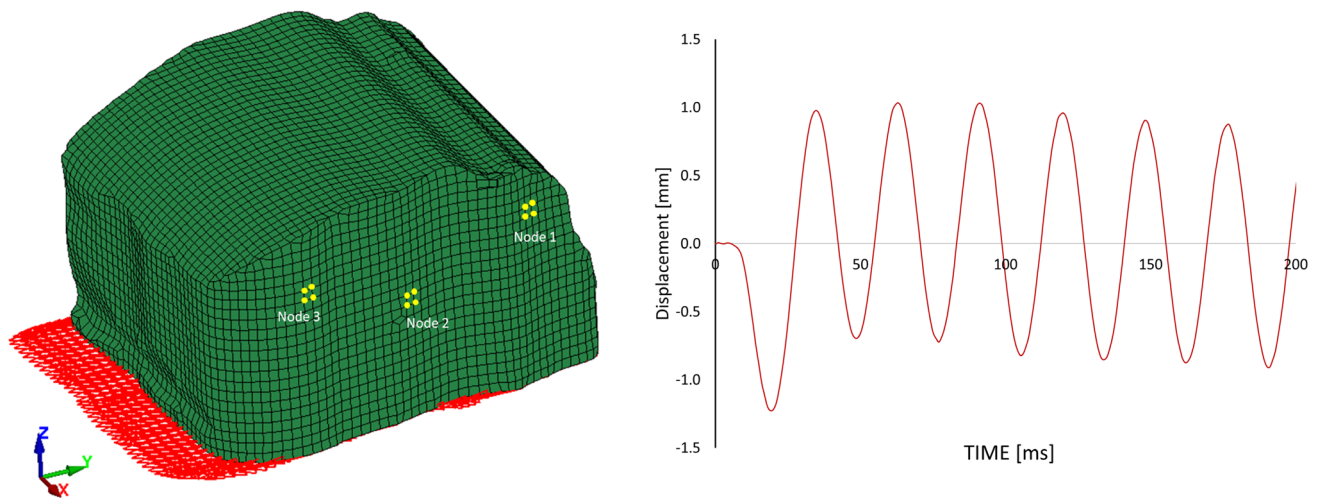


**Fig. 4** Boundary conditions and tracked nodes on the discrete brain sample (left), the amplitude of the base applied as the boundary condition along the Y axis (right)

**Table 1** THUMS material model parameters in LS-DYNA for white matter [41]

Material Model	Parameters
THUMS (Maxwell model)	$\rho = 1000 \text{ kg/m}^3$ $K = 2160 \text{ MPa}$ $G_1 = 6150 \text{ Pa}$ $\beta = 0.06 \text{ s}^{-1}$ $G_o = 12500 \text{ Pa}$

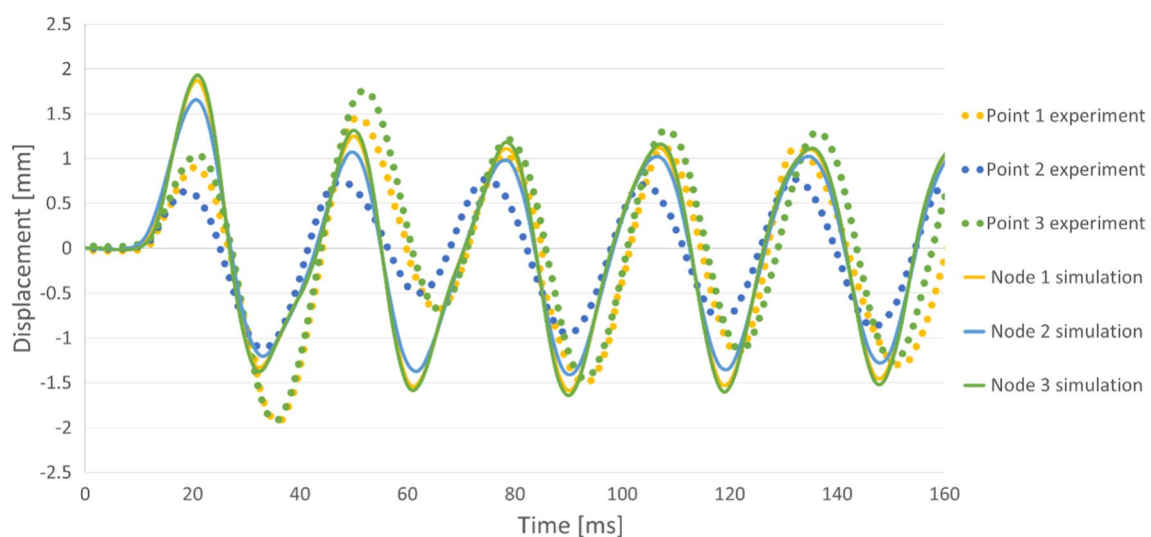
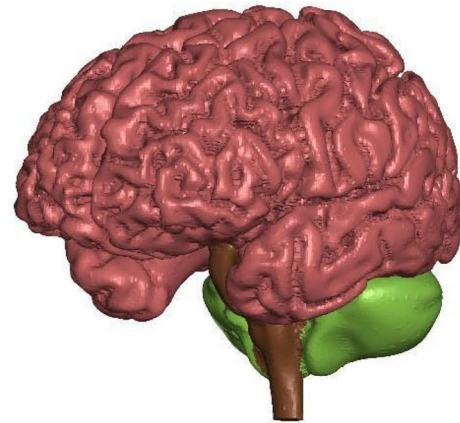


**Fig. 5** Displacement with respect to time for experimental recordings and a numerical simulation for the THUMS mode for the track points/nodes



aHEAD: middle age model

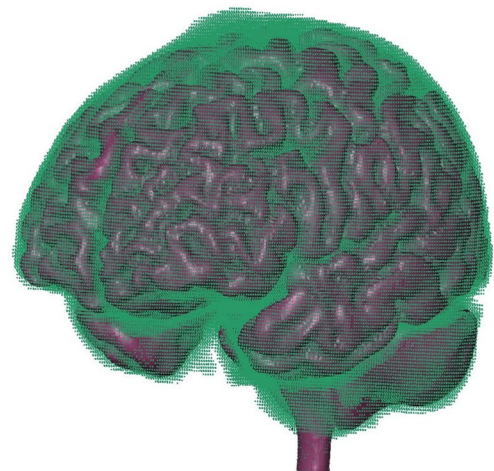
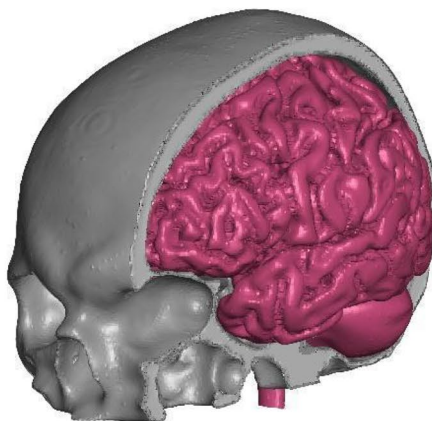
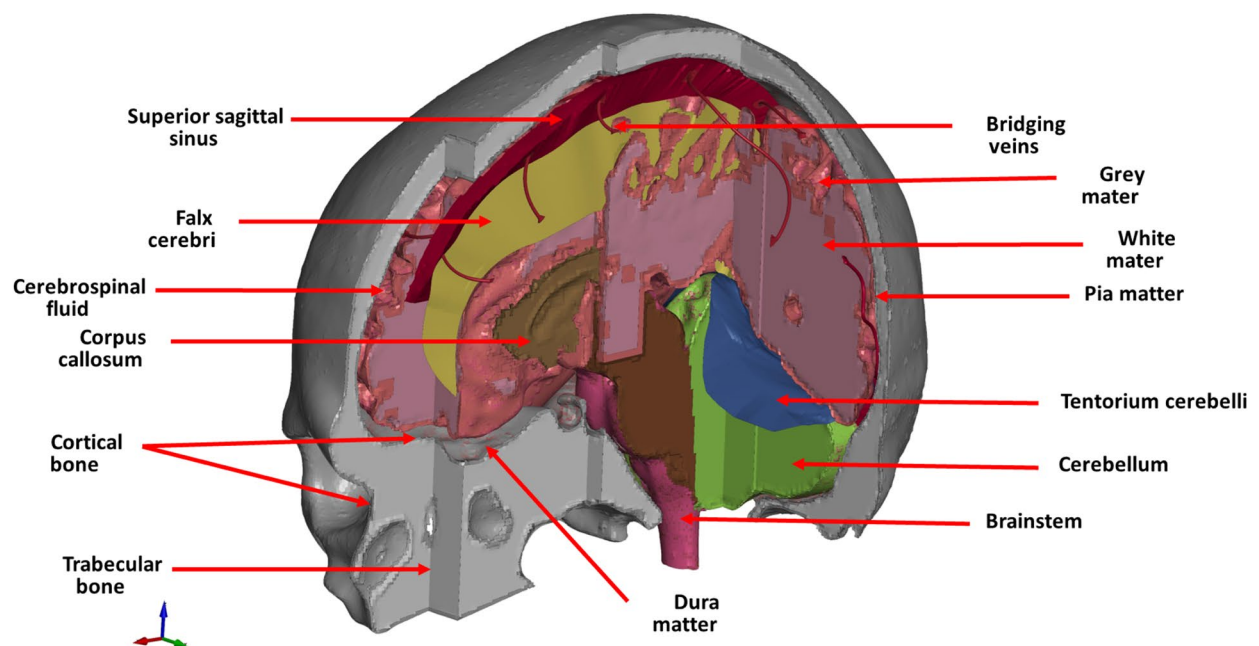


**Fig. 6** aHEAD 28yo discrete model: top-left – CNS structures; top-right – grey matter; cerebellum and brainstem; middle – brain with labelled structures; bottom-left – brain structures inside the skull; bottom-right – CSF and pia mater

and corresponding nodes (#1 and 3), which were tracked more remotely from the base, was higher than those placed closer to the base (point #2). In other words, the closer to the base the more excitation-like displacement with respect to time was observed (Fig. 4 – right). We can explain this by considering the viscoelastic properties of the brain material and the material model in the FE simulation. The material exhibited both viscous and elastic characteristics when undergoing deformation. Interestingly, for some commonly used models of materials in the literature [42–44], we could observe close to rigid-body behaviour (all nodes having a very similar displacement in time), which did not realistically mimic the true nature of the brain tissues [45, 46].

### 2.3 Model construction

Developing a numerical head model from medical imaging is a highly complex task, requiring several stages and approaches. The initial task was to use geometric segmentation on medical images obtained from CT (Computer Tomography), and MRI (Magnetic Resonance Imaging) scanners in DICOM (Digital Imaging and Communications in Medicine) format to obtain the geometry and discretize the model with an FE mesh [47, 48]. Modelling a simplified head can be regarded as a relatively straightforward task for today's CAD/CAE tools [49]. However, increasing the complexity and considering the minor details is tremendously time-consuming work. The developing process can be split into five stages: medical data acquisition and craniometry measurements; CAD – structure segmentation and 3D modelling; FE modelling and material tests; modelling of the complex central nervous system; and, finally, verification tests.

In the first stage, we gathered medical data and extracted the main brain parts, such as the hemispheres, brainstem, cerebellum and skull [24, 50, 51]. Segmentations were made in the 3D Slicer program. Soft structures of the head, such as the brain, are derived from MRI scans. Hard structures, such as the skull, were developed based on computed tomography (CT). Both medical examinations were obtained from the same patient during the same examination – thus, the number of DICOM files was limited.

It should be noted that there are many soft tissues within the brain. In addition, algorithms for recognizing soft human structures are not well developed yet. Therefore, the whole procedure required manual segmentation. This process involved removing isolated and irregular clusters of voxels and performing a stepwise segmentation, starting with the

white matter (WM) selection first and expanding the same section to include the gray matter (GM). However, due to the higher density of bone structures, skull segmentation could be performed with greater use of automatic segmentation algorithms.

The second stage used CAD software such as CATIA and Meshmixer to create 3D geometries based on the medical images. At this point, we combined the geometry of the skull and brain obtained in the segmentation process. Each part was modelled individually, considering the structural segmentation (i.e. white matter – gray matter).

In stage three, the 3D models were transformed into FE software. The emphasis was put on the best element selection as it influenced several simulation details, such as the computational time and result accuracy. It was decided to use hexahedral and quadrilateral elements to remove typical triangular and tetrahedral elements such as a constant-strain triangle [52, 53]. The irregularities and complexity of intracranial structures made commonly used mesh algorithms fail. It was necessary to use robust meshing algorithms from Altair HyperMesh 2019–2021 to generate high-quality, entirely hexahedral meshes for hard and soft tissues that would preserve the unique sulci and gyri geometry. The element size of finite element solids and shells was optimized to approximately 1 mm, which takes recourse on the finest solution of the input for the obtained medical data resolution (DICOM). Some smaller hexahedral elements with a minimum Jacobian value of 0.3 – primarily found at the most outer brain element layers – were used to reflect the complexity of the geometry. Conventional models available on the market represent CSF as hexahedral or tetrahedral solid elements, which is a significant simplification. The aHEAD model employs fluid–structure interaction by SPH representing CSF flow during the impact [29].



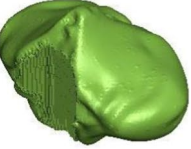

Stage four was dedicated to modelling the intracranial structures of the central nervous system. This action required precise modelling and detailed FE mesh of the superior sagittal sinus, bridging veins and the tentorium cerebelli. The modelling process was based on MRI images and assisted by neurosurgeons. The boundary thickness for the grey matter was established as 2–3 mm. The final aHEAD young adult model is displayed below in Fig. 6.

Since it was not possible to obtain a human body for testing, the final stage was based on validating the model's behaviour under load with the Hardy 755 test [54]. The literature's most frequently used head models are the Global Human Body Models Consortium (GHBMC) and the Total Human Model for Safety (THUMS) models [41, 55]. The grade of detail is very high for a full-body model. However, since there is a stress concentration on the brain's gyri and sulci, the level of detail in the head is not sufficient for advanced brain injury analysis [56, 57]. Moreover, unlike the presented aHEAD model, most available head models

are symmetrical [58]. That is a significant simplification that influences the outcome of the results. The mechanical properties used for the aHEAD 28yo person head model are presented in Table 2 (Appendix A), where  $\nu$  – Poisson's ratio,  $G_0$  – shear modulus,  $G_1$  – Long-time ( $G_\infty$ ) shear modulus,





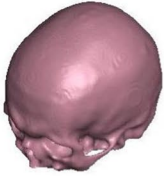



$\mu_1$  – first shear modulus, and  $\alpha_1$  – first exponent for Ogden Rubber (Hyperelastic) model material in LS-DYNA code. The table with each model part and its material properties is included in Appendix A and in the online repository (<https://doi.org/10.5281/zenodo.7503989>).

**Table 2** Mechanical properties of aHEAD 28yo head model

Structure	Reference	Density [kg/m <sup>3</sup> ]	Young's modulus or bulk modulus [MPa]	Other material parameters	Type no. of FEs	Image of structure
White Matter – left/right hemisphere	THUMS MAT_VISCOELASTIC [41]	1000	Bulk modulus 2160	$G_0 = 12500$ Pa $G_1 = 6125$ Pa $\beta = 0.06 \text{ s}^{-1}$	Hexa 398 525/ 419 524	
Grey matter – left/right hemisphere	THUMS MAT_VISCOELASTIC [41]	1000	Bulk modulus 2160	$G_0 = 10000$ Pa $G_1 = 5000$ Pa $\beta = 0.06 \text{ s}^{-1}$	Hexa 237 331/ 213 994	
Cerebellum	Fernandes 2017 [21,59]	1040	–	$\nu = 0.49999$ $\mu_1 = 0.0012$ $\alpha_1 = 5.05007$	Hexa 178 051	
Brainstem	Fernandes 2017 [21,59]	1040	–	$\nu = 0.49999$ $\mu_1 = 0.0012$ $\alpha_1 = 5.05007$	Hexa 41 541	



**Table 2** (continued)

Pia mater	LLC Elemance 2014; Ratajczak et al. 2019 [44,60]	1130	31.5	$\nu = 0.45000$	tri shell 288	
					quad shell 243 677	
Dura mater (with falx cerebri and tentorium cerebelli)	LLC Elemance 2014; Ratajczak et al. 2019 [44,60]	1130	31.5	$\nu = 0.45000$	tri shell 56	
					quad shell 117 540	
Superior sagittal sinus and transversal sinus	LLC Elemance 2014; Ratajczak et al. 2019 [44,60]	1040	28.2	$\nu = 0.45000$	tri shell 130	
					quad shell 10 333	
Bridging veins	Delye et al. 2006; LLC Elemance 2014; Monea et al. 2014 [60–62]	1130	30	$\nu = 0.48000$	tri shell 314	
					quad shell 19 644	
Cortical bone	Giordano and Kleiven 2016; Margulies 2000; Ratajczak et al. 2019 [44,63,64]	2100	4000	$\nu = 0.25000$	hexa 557 384	
Trabecular bone (diploë)	Giordano and Kleiven 2016; Margulies 2000; Ratajczak et al. 2019 [44,63,64]	1000	1000	$\nu = 0.30000$	hexa 573 848	
Cerebrospin al fluid (CSF)	DYNAmore GmbH 2018; Gomez- Gesteira et al. 2012 [65,66]	1000	–	viscosity coefficient $7e-10$	SPH 140 199	
Corpus callosum	Fernandes 2017 [21,59]	1040	<i>Bulk modulus</i> 2160	$G_0 = 6000$ Pa $G_1 = 1200$ Pa $\beta = 80$	hexa 1 8 2 6	

### 3 Results

Following Hardy et al., the simulation boundary conditions were set [38]. The most frequently used test in the literature is the C755-T2 test, which was used in this paper. The test was measured and recorded using a 6-axis accelerometer, which registered both linear and angular acceleration. The output data was registered as six different acceleration functions with respect to time (three translational and three rotational) and was used as an input to the centre of mass in the FE analysis (Fig. 7). The verification of results was based on the relative displacement of ten points placed according to the Hardy test. Note that all the markers except P1 (grey matter) were in the white matter in the numerical model.

The primary purpose of computer simulations is to predict real phenomena. The methods of verification and validation allow the reliability and credibility of computer simulations to be determined and quantified. It should be emphasized that the computational model is a discretized approximation of a mathematical model. Validation is the process of checking to what extent the FEM model represents a real phenomenon (biological object) from the point of view of the future application of this model in practice. However, due to the lack of experimental data, validating the numerical model is a serious problem in computational mechanics. In the literature in the field of brain mechanics, there are few descriptions of experimental studies carried out on dissection preparations of human cadavers, which allow the numerical models to be related to these data. Currently, in the literature, one of the best-described experimental

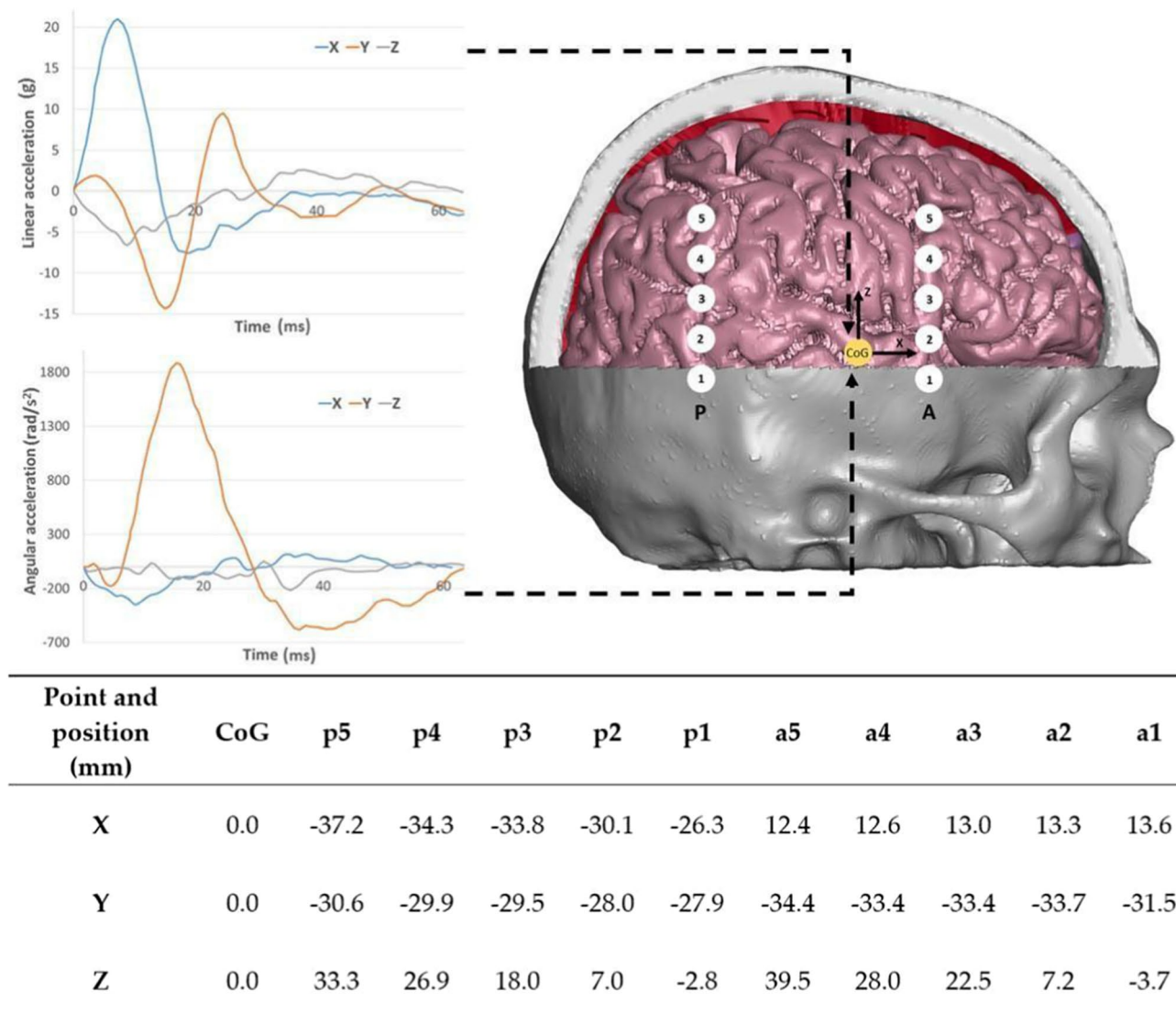


Fig. 7 Hardy C755-T2 test boundary conditions

studies of the influence of external forces on the response of human brain tissues is that by Hardy et al. [38]. The essence of this study was to analyze the displacement of the brain in relation to the skull. It can be observed in the literature that this experiment is one of the most frequently used tests for the verification of numerical head models.

The above Fig. 8 depicts the comparison between the experimental and numerical neutral density targets (NDTs) relative displacement in both the X and Z directions. We need to highlight here that the results differ significantly, particularly for the last segment of the impact, to the relatively high displacements reached with the FE model. For the posterior column, the displacement history was similar for the first 30 ms in the X-direction and approximately the same for the first 20 ms in the Z-direction. A similar pattern was observed for the anterior column in the X-direction, although the magnitude in the first 30 ms was much higher in the simulations and increased excessively afterwards. The NDTs in the anterior column, in the Z-direction, did not follow this pattern and were closer to Hardy's experiment.

Considering the level of detail of our model and multivariate material testing, these findings are surprising – mainly because several models are available in the literature that successfully attempted the validation against Hardy's experiments. In comparison, other FE models available on the market have simpler geometries (without sulci and gyri structures), employ linear elastic constitutive laws, and use solid FE elements to model fluids, such as CSF, often using lower-quality tetrahedral elements. The authors hypothesize about how easy it is to shift the overall behaviour of the

entire model with fluid representation using solid elements. The overall stiffness of the model highly influences brain displacement.

## 4 Discussion

The development of human body models requires performing validation tests or parallel testing to ensure that the assumptions employed are valid and adequate. Thus, the authors decided to use porcine brain tissue from commercial suppliers, which is not covered by the bio-ethical code of conduct, to perform parallel testing of material models. The use of a vibration test with a high-speed camera allowed us to create benchmarks between the numerical model and physical specimens. It turned out that many models of materials applied in LS-DYNA and Abaqus CAE that we tested behave as rigid bodies, unlike the viscoelastic brain tissues (see repository (<https://doi.org/10.5281/zenodo.7503989>)).

The displacement achieved at the end of the simulation for Hardy's test, particularly in the posterior column and for both components, was higher than the experimental data. Since additional novel validation of the material model was carried out, and the model presented highly detailed geometries, the potential issue might have been related to SPH formulation. It was observed that the higher the distance between the NDT and the CoG, the higher the displacement. The authors assume that SPH formulation played a role in the deformation mechanism. The untypical level of CSF was also noticed in the images from Hardy's C755-T2

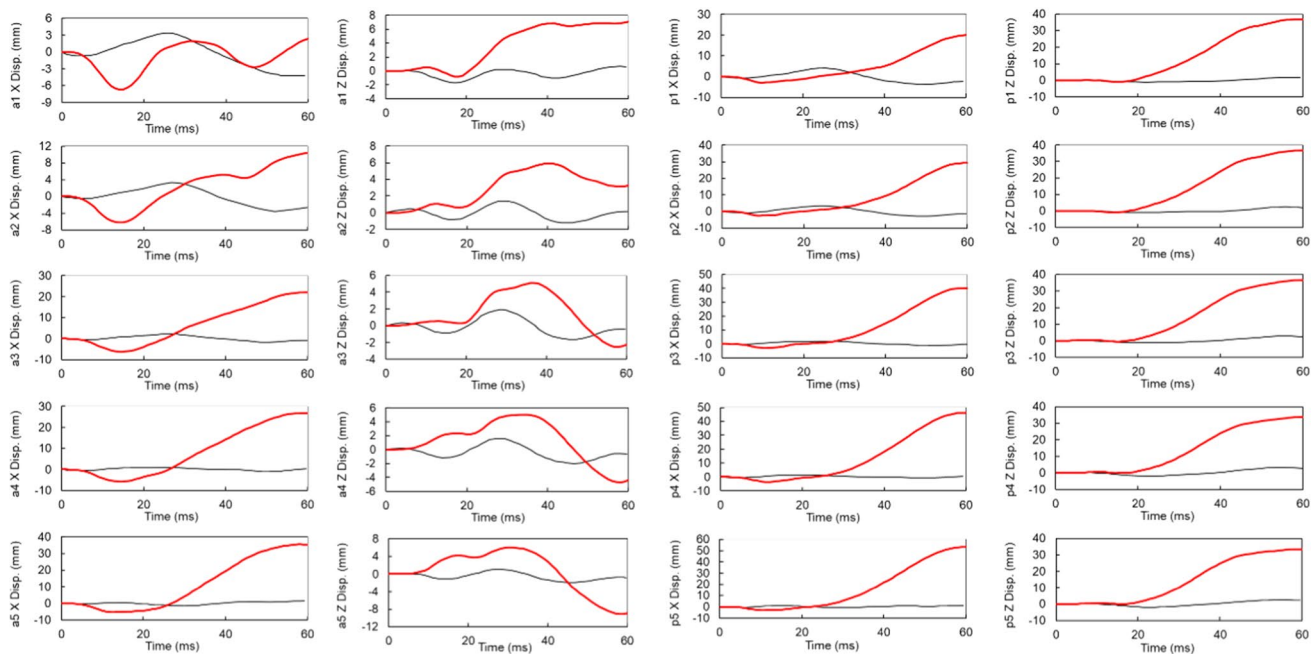


**Fig. 8** Hardy C755-T2 test results with FEM simulation curves for aHEAD 28yo head model

experiment. However, it was reported that the level of CSF in the cadaver's head was kept at a constant level. Hardy conducted an experiment with an unprecedented degree of meticulousness in preparing the specimen. The head, as well as the cervical and a part of the thoracic spine, were detached from the body, and after removing the spinal cord part, the dural sac was sealed. Perfusion through the carotid arteries and jugular veins was facilitated with an artificial CSF. The vertebral arteries were left patent to ensure the removal of air from the vessels. This preparation left no significant amount of air in the vasculature, but there is a concern about the ventricular system. Almost always, after cutting an opening the dural sac, some air enters its lumen and migrates to the lateral ventricles of the brain. In the X-ray scan of the specimen with attached measuring equipment (Fig. 9), supposedly taken just before the experiment, there might be visible a bubble of air in the lateral ventricles—marked as a blue arrow in Fig. 9. For the proper orientation, the ground level during the scan was marked in blue.

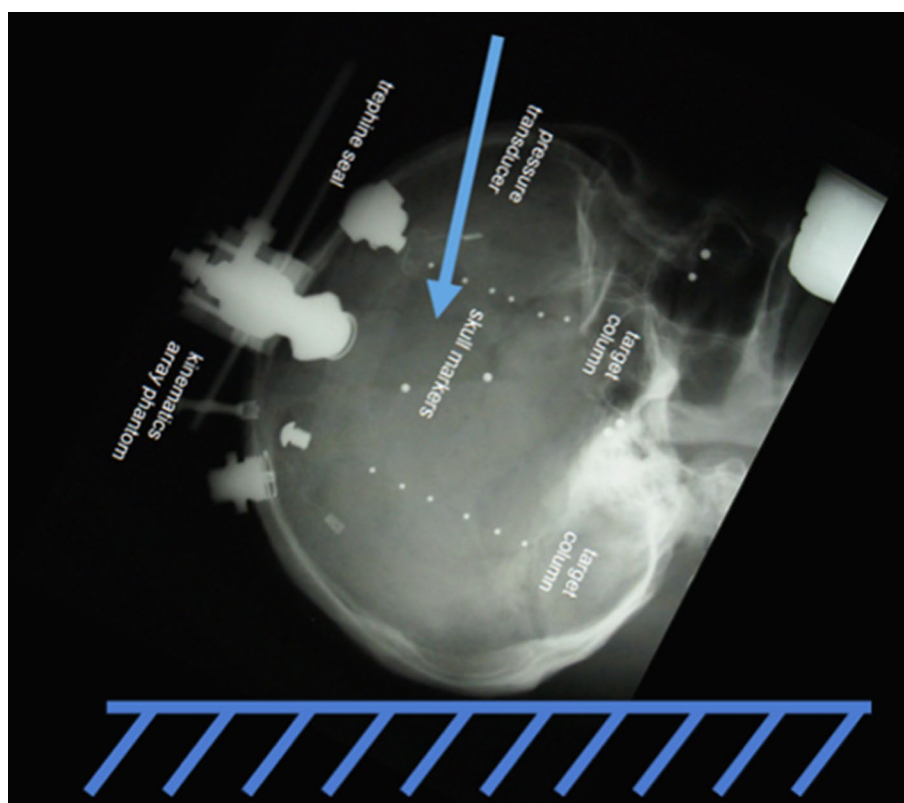
The authors think one of the most significant achievements in the presented FEM is the use of SPH for CSF. The density was set to  $1e^{-6} \text{kg}/\text{m}^3$  and the viscosity coefficient to  $7e^{-10}$ , which matched the fluid properties. The number of particles was set to approximately 140,000. This approach allowed the particles to move freely, representing the CSF in the human skull. This is impossible for artificial CSF

modelled as incompressible solid elements prone to shear-locking phenomena. The particles interact with the structural FEs using a penalty-based contact definition. There are some published studies with CSF modelled by SPH. However, the studies implemented a simplified brain model and were based on Hardy's physical testing [29, 67]. Numerous research groups, such as Madhukar [68], Duckworth [69] Rycman [70] et al. have proved that SPH can be successfully used in the representation of CSF.

Brain tissue material testing is still an open question in science. Mechanical models and properties are far from each other, and no solid standards or guidelines are acknowledged by the scientific community in this field. New approaches have been proposed by various authors. The most dominant material testing approach is quasi-static compression, eventually tension. In this paper, the authors assumed that viscoelastic material should reveal its properties during cycling load conditions. Those boundary conditions showed that static material tests miss several aspects of the brain tissue behaviour.

However, it should be noted that our results do not fit Hardy's test results, as do these FE head models, where tetrahedral FEs or merged brain-to-skull formulations were employed. This discrepancy cannot be treated as a disqualification for any of these tests. From the start of our research, we tried to establish a logical path for the series of experiments that are described in the paper, revealing all the

**Fig. 9** A potential air bubble in the lateral ventricles (blue arrow), reproduced from [54]





material data used in the simulations. We believe that data tuning to obtain a better fit to Hardy's results is a violation of scientific ethics. At this stage, the discrepancy of displacement results is clearly visible, yet the authors would like to strongly encourage scientists to discuss these differences and make a conclusion as to what might be the source of them. The most desirable solution would be to conduct some new cadaver tests. However, the European national rules are very strict regarding cadaver testing. The budget and possibilities of the project have not allowed the authors to proceed with cadaver head experiments. Currently, the solution is to compare the displacements of selected points from Hardy's experiment with numerical results. With the technology continuously developing, it is suggested to prepare new experiments and investigate brain behaviour under specific loading, such as the one published by Alshareef et al. [71].

## 5 Final conclusion

The article is focused on an innovative material testing approach for a new generation of FE head models based on quality numerical mesh and CSF modelled as mesh-free to mimic the real fluid behaviour during high mechanical loading. Taking into account the extensive literature reviews in the field of numerical modelling, it can be noted that the developed numerical model is highly complex. The space for CSF was filled using an SPH method, and this approach allowed the CSF to have complex dynamics. In addition, the aHEAD model consisted only of hexahedral elements for 3D structures.

Experimental studies are an essential advantage of this paper. Currently, there are significant discrepancies in the literature on the results of experimental brain tissue tests. Standard tests include stretching or compression of the samples. To date, the current validation of numerical models consists mainly of comparing acceleration and deflection force diagrams for fall and compression tests. Nevertheless, bearing in mind the structure of the brain and the nature of the brain tissue material, the authors decided to conduct tests with oscillation displacement. The vibration tests are much closer to the actual brain mechanical loading. Additional trackers had to be applied on the specimen to provide characteristic points for the motion analysis and digital image correlation. Nonetheless, the presented method has several limitations, which are covered in the relevant sections dedicated to the challenges related to non-contact measurement methods. Finally, the numerical simulation based on physical experiments proved that the brain material model used in THUMS, among the other tested, is valid for the given boundary conditions.

The second part of the study presents the aHEAD numerical head model developed to mimic the brain of a young

adult human. A high-detail geometrical representation characterizes the model. Surprisingly, the Hardy C755-T2 validation test results differed from the experiment. However, the authors presented a logical path for a series of experiments to validate the material model used in numerical simulations. We also highlighted some important issues in Hardy's experiments—the CSF infill in the cadaver's skull might be a factor which influenced the displacement curves depicted in this study. As many researchers treat Hardy's tests as a benchmark, this issue will be explicitly verified. Moreover, extensive cadaveric or tissue tests will be performed. Since these kinds of studies are very rare, mainly due to ethical concerns and cost burden, some new techniques and methods, such as the ones described in this study, will be further developed to bridge the gaps in the state-of-the-art.

To conclude—the main goal of this work was achieved by developing a comprehensive model of the human head, addressing the non-linear material behaviour of both soft and hard tissues, as well as complex material interactions. There is a complete sulci and gyri geometry, pressurized bridging veins represented by 2D elements, and CSF represented by the SPH particles. All 3D structures are represented only with hexahedral finite elements. Moreover, relevant to achieve such a goal was the novel comprehensive experimental-computational approach validating the numerical model at the tissue level. The developed model, along with its double verification tests (tissue-level and Hardy experimental cadaver test), aims to establish a benchmark in numerical head modelling and can provide some new insights into computational injury biomechanics.

## Appendix A

### Digital image correlation approach

The strain measurements with respect to highly elastic materials are still a current scientific problem. Finite strain assumptions are no longer valid for such complicated cases as human brain tissue where axial anisotropy, not void-free and not homogenous material is present with hyper-visco-elastic behaviour. Thus a non-contact measurement method is used. Digital Image Correlation (DIC) is a technique which allows the measurement of strain fields based on the movement of clusters of pixels in the sequence of pictures or frames. With two cameras setup, it is possible to obtain a three-dimensional strain field, whereas a single camera setup allows obtaining a plain strain field. In our approach, a single camera setup was used with a 45° mirror which allowed us to record two perpendicular sides of a specimen in one picture

(Fig. 10). Due to the vibration movement of the excitation, a high-speed camera was used to record several frames of the test bench with specimens in half of the cycle—between two extreme positions.

It needs to be underlined that these measurements are not precise due to the post-processing of collected records, which allowed us to perform only quantitative analysis. In the limitations subchapter, the authors described precisely which factors lead to unsuccessful strain field calculations. At this stage, we want to share

this idea of measurements with other researchers even if mixed quality has been obtained so far. The python scripts used in the experiment are available in the online repository referred in the manuscript. The summary of all tested samples is presented in Table 3.

See (Table 3).

**See Fig. 10**

**Table 3** A summary of all tested samples

Sample number		Mass [g]	Volume [ml]	Frquency 1st [Hz]	Frquency 2nd [Hz]
Sample 1	Medulla	2.1	2	35–45	–
Sample 2	Medulla	2.4	2.25	35–45	–
Sample 3	Cerebellum	3.5	3.5	35–45	60–100
Sample 4	Hemisphere	2.1	2	35–45	60–100
Sample 4	Hemisphere	1.9	1.5	35–45	60–100
Sample 6	Cerebellum	1.5	1.5	35–45	200–1000
Sample 7	Medulla	1	1	60–100	–
Sample 8	Medulla	1.1	1	35–45	60–100
Sample 9	Brain Nuclei	2.2	2	35–45	–
Sample 10	Hemisphere	6.5	6.5	35–45	–
Sample 11	Hemisphere	7.1	7	60–100	–

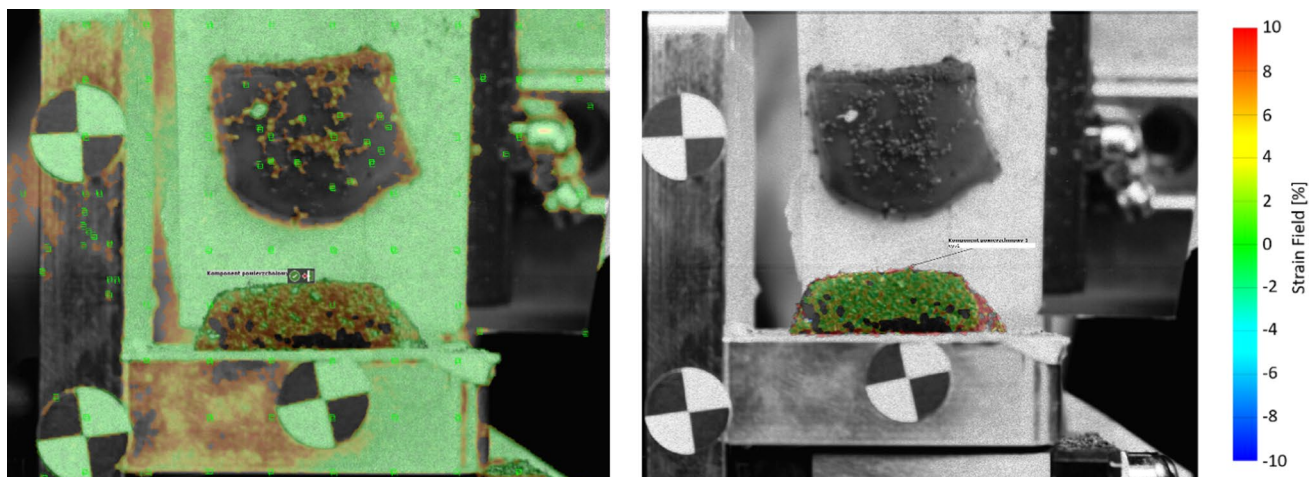


**Fig. 10** Digital image correlation: on the left – quality assessment of the picture, on the right – specimen's strain field

**Funding** This research was co-funded by the National Centre for Research and Development of Poland, grant number LIDER/8/0051/L-8/16/NCBR/2017. [www.aheadproject.org](http://www.aheadproject.org). Moreover, some of the authors would like to acknowledge the support from NAWA STER Program Internationalization of Wroclaw University of Science and Technology Doctoral School.

**Data availability** Additional data is available in an online repository: <https://doi.org/10.5281/zenodo.7503989> and <https://www.youtube.com/@aheadproject6533/videos>.

## Declarations

**Conflict of interest** The authors declare no conflict of interest.

**Ethical approval** Ethical review and approval were not required for the study on human participants in accordance with the local legislation and institutional requirements. Moreover, written informed consent for participation was not needed for this study in accordance with national legislation and institutional requirements as the data was anonymised. No living animal studies are presented in the manuscript.

**Open Access** This article is licensed under a Creative Commons Attribution 4.0 International License, which permits use, sharing, adaptation, distribution and reproduction in any medium or format, as long as you give appropriate credit to the original author(s) and the source, provide a link to the Creative Commons licence, and indicate if changes were made. The images or other third party material in this article are included in the article's Creative Commons licence, unless indicated otherwise in a credit line to the material. If material is not included in the article's Creative Commons licence and your intended use is not permitted by statutory regulation or exceeds the permitted use, you will need to obtain permission directly from the copyright holder. To view a copy of this licence, visit <http://creativecommons.org/licenses/by/4.0/>.

## References

- Maas AIR, Menon DK, Adelson PD, et al. Traumatic brain injury: integrated approaches to improve prevention, clinical care, and research. *Lancet Neurol*. 2017;16:987–1048. [https://doi.org/10.1016/S1474-4422\(17\)30371-X](https://doi.org/10.1016/S1474-4422(17)30371-X).
- James SL, Theadom A, Ellenbogen RG, et al. Global, regional, and national burden of traumatic brain injury and spinal cord injury, 1990–2016: a systematic analysis for the global burden of disease study 2016. *Lancet Neurol*. 2019;18:56–87. [https://doi.org/10.1016/S1474-4422\(18\)30415-0](https://doi.org/10.1016/S1474-4422(18)30415-0).
- Te Ao B, Brown P, Tobias M, Ameratunga S, Barker-Collo S, Theadom A, McPherson K, Starkey N, Dowell A, Jones K, Feigin VL. Cost of traumatic brain injury in New Zealand: evidence from a population-based study. *Neurology*. 2014;83:1645–52. <https://doi.org/10.1212/WNL.0000000000000933>.
- Bastien C, Neal-Sturgess C, Davies H, Cheng X. Computing brain white and grey matter injury severity in a traumatic fall. *Math Comput Appl*. 2020;25:61. <https://doi.org/10.3390/mca25030061>.
- Fernandes FAO, Alves de Sousa RJ, Ptak M, Wilhelm J. Certified motorcycle helmets: computational evaluation of the efficacy of standard requirements with finite element models. *Math Comput Appl*. 2020;25:12. <https://doi.org/10.3390/mca25010012>.
- Baghaei SM, Sadegh AM, Charles S. Characteristics of HIC in prediction of mTBI relating to crash pulses. *Int J Veh Des*. 2019;80:59. <https://doi.org/10.1504/IJVD.2019.105066>.
- Fernandes F, Alves de Sousa R, Ptak M, Migueis G. Helmet design based on the optimization of biocomposite energy-absorbing liners under multi-impact loading. *Appl Sci*. 2019;9:735. <https://doi.org/10.3390/app9040735>.
- Li S, Xiao Z, Zhang Y, Li QM. Impact analysis of a honeycomb-filled motorcycle helmet based on coupled head-helmet modelling. *Int J Mech Sci*. 2021;199:106406. <https://doi.org/10.1016/j.jimecsci.2021.106406>.
- Toma M, Nguyen PDH. Coup-contrecoup brain injury: fluid-structure interaction simulations. *Int J Crashworthiness*. 2020;25:175–82. <https://doi.org/10.1080/13588265.2018.1550910>.
- Dmitruk A, Naplocha K, Pach J, Pyka D, Ziółkowski G, Bocian M, Jamrozik K. Experimental and numerical study of ballistic resistance of composites based on sandwich metallic foams. *Appl Compos Mater*. 2021;28:2021–44. <https://doi.org/10.1007/s10443-021-09957-0>.
- Dymek M, Ptak M, Fernandes FAO. Design and virtual testing of american football helmets—a review. *Arch Comput Methods Eng*. 2021;29:1277–89. <https://doi.org/10.1007/s11831-021-09621-7>.
- Rawska K, Gepner B, Kerrigan JR. Effect of various restraint configurations on submarining occurrence across varied seat configurations in autonomous driving system environment. *Traffic Inj Prev*. 2021;22:S128–33. <https://doi.org/10.1080/15389588.2021.1939872>.
- Varela MM, Fernandes FAO, Alves de Sousa RJ. Development of an eco-friendly head impact protection device. *Appl Sci*. 2020;10:2492. <https://doi.org/10.3390/app10072492>.
- Forman J, Miller M, Perez-Rapela D, Gepner B, Edwards MA, Jermakian JS. Investigation of factors influencing submarining mitigation with child booster seats. *Traffic Inj Prev*. 2022. <https://doi.org/10.1080/15389588.2022.2153594>.
- Wdowicz D, Ptak M. Numerical approaches to pedestrian impact simulation with human body models: a review. *Arch Comput Methods Eng*. 2023. <https://doi.org/10.1007/s11831-023-09949-2>.
- Dixit P, Liu GR. A review on recent development of finite element models for head injury simulations. *Arch Comput Methods Eng*. 2017;24:979–1031. <https://doi.org/10.1007/s11831-016-9196-x>.
- Fernandes FAO, Alves de Sousa RJ, Ptak M. Finite element head modelling and head injury predictors. *Head Inj Simulat Road Traf Acc*. 2018. [https://doi.org/10.1007/978-3-319-89926-8\\_1](https://doi.org/10.1007/978-3-319-89926-8_1).
- Giudice JS, Zeng W, Wu T, Alshareef A, Shedd DF, Panzer MB. An analytical review of the numerical methods used for finite element modeling of traumatic brain injury. *Ann Biomed Eng*. 2019;47:1855–72. <https://doi.org/10.1007/s10439-018-02161-5>.
- Madhukar A, Ostojic-Starzewski M. Finite element methods in human head impact simulations: a review. *Ann Biomed Eng*. 2019. <https://doi.org/10.1007/s10439-019-02205-4>.
- Wang Q, Lou Y, Li T, Jin X. Development and application of digital human models in the field of vehicle collisions: a review. *Ann Biomed Eng*. 2021;49:1619–32. <https://doi.org/10.1007/s10439-021-02794-z>.
- Fernandes FAO, Tchepel D, Alves de Sousa RJ, Ptak M. Development and validation of a new finite element human head model. *Eng Comput*. 2018;35:477–96. <https://doi.org/10.1108/EC-09-2016-0321>.
- Zhao W, Ford JC, Flashman LA, McAllister TW, Ji S. White matter injury susceptibility via fiber strain evaluation using whole-brain tractography. *J Neurotrauma*. 2016;33:1834–47. <https://doi.org/10.1089/neu.2015.4239>.
- Zhou Z, Wang T, Jörgens D, Li X. Fiber orientation downsampling compromises the computation of white matter tract-related deformation. *J Mech Behav Biomed Mater*. 2022;132:105294. <https://doi.org/10.1016/j.jmbbm.2022.105294>.
- Wilhelm J, Ptak M, Fernandes FAO, Kubicki K, Kwiatkowski A, Ratajczak M, Sawicki M, Szarek D. Injury biomechanics of a child's head: problems, challenges and possibilities with a new




- aHEAD finite element model. *Appl Sci.* 2020;10:4467. <https://doi.org/10.3390/app10134467>.
25. Fernandes FAO, de Alves Sousa RJ, Ptak M. Validation of YEAHM. Springer briefs application science technology. New York: Springer; 2018. p. 41–58. [https://doi.org/10.1007/978-3-319-89926-8\\_3](https://doi.org/10.1007/978-3-319-89926-8_3).
26. Weickenmeier J, Saez P, Butler CAM, Young PG, Goriely A, Kuhl E. Bulging brains. *J Elast.* 2017;129:197–212. <https://doi.org/10.1007/s10659-016-9606-1>.
27. Zhou Z, Li X, Liu Y, Hardy WN, Kleiven S. Brain strain rate response: addressing computational ambiguity and experimental data for model validation. *Brain Multiphysics.* 2023;4:100073. <https://doi.org/10.1016/j.brain.2023.100073>.
28. Jin JX, Zhang JY, Song XW, Hu H, Sun XY. Numerical simulation of fluid-structure interaction relations between skull and brain based on ALE and overlapping mesh methods. *Appl Mech Mater.* 2015;713–715:1782–5. <https://doi.org/10.4028/www.scientific.net/AMM.713-715.1782>.
29. Toma M, Nguyen PDH. Fluid–structure interaction analysis of cerebrospinal fluid with a comprehensive head model subject to a rapid acceleration and deceleration. *Brain Inj.* 2018;32:1576–84. <https://doi.org/10.1080/02699052.2018.1502470>.
30. Zhou Z, Li X, Kleiven S. Fluid–structure interaction simulation of the brain–skull interface for acute subdural haematoma prediction. *Biomech Model Mechanobiol.* 2019;18:155–73. <https://doi.org/10.1007/s10237-018-1074-z>.
31. Toma M, Chan-Akeley R, Lipari C, Kuo S-H. Mechanism of coup and contrecoup injuries induced by a knock-out punch. *Math Comput Appl.* 2020;25:22. <https://doi.org/10.3390/mca25020022>.
32. Hu J. Parametric human modeling. In: Hu J, editor. Basic finite element method as applied to injury biomechanics. New York: Elsevier; 2018.
33. Im K, Lee J-M, Lyttelton O, Kim SH, Evans AC, Kim SI. Brain size and cortical structure in the adult human brain. *Cereb Cortex.* 2008;18:2181–91. <https://doi.org/10.1093/cercor/bhm244>.
34. Singh D, Boakye-Yiadom S, Cronin DS. Comparison of porcine brain mechanical properties to potential tissue simulant materials in quasi-static and sinusoidal compression. *J Biomech.* 2019;92:84–91. <https://doi.org/10.1016/j.jbiomech.2019.05.033>.
35. Costa JMC, Fernandes FAO, Alves de Sousa RJ. Prediction of subdural haematoma based on a detailed numerical model of the cerebral bridging veins. *J Mech Behav Biomed Mater.* 2020;111:103976. <https://doi.org/10.1016/j.jmbbm.2020.103976>.
36. Zhao W, Ji S. Incorporation of vasculature in a head injury model lowers local mechanical strains in dynamic impact. *J Biomech.* 2020;104:109732. <https://doi.org/10.1016/j.jbiomech.2020.109732>.
37. W.N. Hardy, C.D. Foster, M.J. Mason, K.H. Yang, A.I. King, S. Tashman, Investigation of head injury mechanisms using neutral density technology and high-speed biplanar X-ray, In: SAE Tech. Pap. SAE International. 2001. Doi: <https://doi.org/10.4271/2001-22-0016>.
38. Hardy WN, Mason MJ, Foster CD, Shah CS, Kopacz JM, Yang KH, King AI, Bishop J, Bey M, Anderst W, Tashman S. A study of the response of the human cadaver head to impact. *Stapp Car Crash J.* 2007;51:17–80.
39. Livermore Software Technology Corporation (LSTC), LS-DYNA keyword user's manual vol. 1, Livermore, 2007.
40. Yu C, Wang F, Wang B, Li G, Li F. A computational biomechanics human body model coupling finite element and multibody segments for assessment of head/brain injuries in car-to-pedestrian collisions. *Int J Environ Res Public Health.* 2020;17:492. <https://doi.org/10.3390/ijerph17020492>.
41. Dyna More, Human Model - Total HUMAN Model for Safety THUMS v 4.0, (2012). <http://www.dynamore.de/en/products/models/human> 11/05/12 (Accessed 11 May 2012).
42. Mendis KK, Stalnaker RL, Advani SH. A constitutive relationship for large deformation finite element modeling of brain tissue. *J Biomech Eng.* 1995;117:279–85.
43. Patton DA, McIntosh AS, Kleiven S. The biomechanical determinants of concussion: finite element simulations to investigate brain tissue deformations during sporting impacts to the unprotected head. *J Appl Biomech.* 2013;29:721–30.
44. Ratajczak M, Ptak M, Chybowski L, Gawdzińska K, Będziński R. Material and structural modeling aspects of brain tissue deformation under dynamic loads. *Materials (Basel).* 2019;12:271. <https://doi.org/10.3390/ma12020271>.
45. Wan Y, Fawzi AL, Kesari H. Determining rigid body motion from accelerometer data through the square-root of a negative semi-definite tensor, with applications in mild traumatic brain injury. *Comput Methods Appl Mech Eng.* 2022;390:114271. <https://doi.org/10.1016/j.cma.2021.114271>.
46. MacManus DB, Ghajari M. Material properties of human brain tissue suitable for modelling traumatic brain injury. *Brain Multiphysics.* 2022;3:100059. <https://doi.org/10.1016/j.brain.2022.100059>.
47. Migueis GFJ, Fernandes FAO, Ptak M, Ratajczak M, Alves de Sousa RJ. Detection of bridging veins rupture and subdural haematoma onset using a finite element head model. *Clin Biomech.* 2019;63:104–11. <https://doi.org/10.1016/j.clinbiomech.2019.02.010>.
48. Z. Zhou. Evaluation of Fluid-Structure Interaction and Biofidelity of Finite Element Head Models. 2019.
49. Jona G, Furman-Haran E, Schmidt R. Realistic head-shaped phantom with brain-mimicking metabolites for 7 T spectroscopy and spectroscopic imaging. *NMR Biomed.* 2021. <https://doi.org/10.1002/nbm.4421>.
50. W. Wolański, E. Krawlewska, D. Larysz, M. Gzik, J. Gorwa, R. Michnik, 2019 Prediction of the Child's Head Growth in the First Year of Life, In: W. Wolański (ed) ECCOMAS Thematic Conference on Computational Vision and Medical Image Processing 2019 Porto. Portugal Doi: [https://doi.org/10.1007/978-3-030-32040-9\\_28](https://doi.org/10.1007/978-3-030-32040-9_28).
51. Mazurkiewicz L, Baranowski P, Karimi HR, Damaziak K, Malachowski J, Muszynski A, Muszynski A, Robbersmyr KG, Vangi D. Improved child-resistant system for better side impact protection. *Int J Adv Manuf Technol.* 2018;97:3925–35. <https://doi.org/10.1007/s00170-018-2236-y>.
52. Yang KH. Isoparametric formulation and mesh quality. Basic finite element method as applied to injury biomechanics. New York: Elsevier; 2018. <https://doi.org/10.1016/B978-0-12-809831-8.00003-9>.
53. Rusiński E, Czmochoński J, Smolnicki T. Advanced finite element method for load-carrying structures of machines. Wrocław: Publishing House of Wrocław University of Technology; 2000.
54. Hardy WN. Response of the human cadaver head to impact. Detroit: Wayne State University; 2007.
55. GHMBC, LLC, User Manual: M50 Occupant Version 4.2 for LS-DYNA. (2014).
56. Ghajari M, Hellyer PJ, Sharp DJ. Computational modelling of traumatic brain injury predicts the location of chronic traumatic encephalopathy pathology. *Brain.* 2017;140:333–43. <https://doi.org/10.1093/brain/aww317>.
57. Fischl B. FreeSurfer. *Neuroimage.* 2012;62:774–81. <https://doi.org/10.1016/j.neuroimage.2012.01.021>.
58. Ratajczak M, Ptak M, Kwiatkowski A, Kubicki K, Fernandes FAO, Wilhelm J, Dymek M, Sawicki M, Żółkiewski S. Symmetry of the human head—are symmetrical models more applicable in numerical analysis? *Symmetry (Basel).* 2021;13:1–15. <https://doi.org/10.3390/sym13071252>.
59. Fernandes FAO. Análise biomecânica de impactos com capacetes: novos materiais e geometrias, biomechanical analysis of helmeted



- head impacts: novel materials and geometries. Aveiro: Universidade de Aveiro; 2017.
60. LLC Elemance, Global Human Body Models Consortium, User Man. M50 Occupant Version 4.2 LS-DYNA. (2014).
  61. Monea AG, Van der Perre G, Baek K, Delye H, Verschueren P, Forausebergher E, Van Lierde C, Verpoest I, Vander Sloten J, Goffin J, Depreitere B. The relation between mechanical impact parameters and most frequent bicycle related head injuries. *J Mech Behav Biomed Mater*. 2014;33:3–15. <https://doi.org/10.1016/j.jmbbm.2013.06.011>.
  62. Delye H, Goffin J, Verschueren P, Vander Sloten J, Van der Perre G, Alaerts H, Verpoest I, Berckmans D. Biomechanical properties of the superior sagittal sinus-bridging vein complex. *Stapp Car Crash J*. 2006;50:625–36.
  63. Margulies SS. Infant skull and suture properties: measurements and implications for mechanisms of pediatric brain injury. *J Biomech Eng*. 2000;122:364. <https://doi.org/10.1115/1.1287160>.
  64. C. Giordano, S. Kleiven, (2016) Development of a 3-Year-Old Child FE Head Model, Continuously Scalable from 1.5- to 6-Year-Old, IRCOB Conf. 288–302.
  65. Gomez-Gesteira M, Crespo AJC, Rogers BD, Dalrymple RA, Dominguez JM, Barreiro A. SPHysics—development of a free-surface fluid solver—part 2: efficiency and test cases. *Comput Geosci*. 2012;48:300–7. <https://doi.org/10.1016/j.cageo.2012.02.028>.
  66. DYNAmore GmbH, LS-DYNA Examples, wave-structure interaction. (2018).
  67. Toma M, Dehesa-Baeza A, Chan-Akaley R, Nguyen PDH, Zwi- bel H. Cerebrospinal fluid interaction with cerebral cortex during pediatric abusive head trauma. *J Pediatr Neurol*. 2020;18:223–30. <https://doi.org/10.1055/s-0040-1708495>.
  68. Madhukar A, Chen Y, Ostojka-Starzewski M. Effect of cerebrospinal fluid modeling on spherically convergent shear waves during blunt head trauma. *Int J Numer Method Biomed Eng*. 2017. <https://doi.org/10.1002/cnm.2881>.
  69. Duckworth H, Sharp DJ, Ghajari M. Smoothed particle hydrodynamic modelling of the cerebrospinal fluid for brain biomechanics: accuracy and stability. *Int j Numer Method Biomed Eng*. 2021. <https://doi.org/10.1002/cnm.3440>.
  70. Rycman A, McLachlin S, Cronin DS. Comparison of numerical methods for cerebrospinal fluid representation and fluid–structure interaction during transverse impact of a finite element spinal cord model. *Int J Numer Method Biomed Eng*. 2022. <https://doi.org/10.1002/cnm.3570>.
  71. Alshareef A, Giudice JS, Forman J, Salzar RS, Panzer MB. A novel method for quantifying human in situ whole brain deformation under rotational loading using sonomicrometry. *J Neurotrauma*. 2018;35:780–9. <https://doi.org/10.1089/neu.2017.5362>.

**Publisher's Note** Springer Nature remains neutral with regard to jurisdictional claims in published maps and institutional affiliations.

## Authors and Affiliations

Mariusz Ptak<sup>1</sup>  · Mateusz Dymek<sup>1</sup>  · Marek Sawicki<sup>1</sup>  · Fábio A. O. Fernandes<sup>2</sup>  · Maciej Wnuk<sup>1</sup> · Johannes Wilhelm<sup>3</sup>  · Monika Ratajczak<sup>4</sup>  · Daria Witkowska<sup>5</sup>  · Artur Kwiatkowski<sup>6</sup> · Błażej Poźniak<sup>7</sup>  · Konrad Kubicki<sup>8</sup> · Marta Tikhomirov<sup>9</sup>  · Adam Druszczyk<sup>6</sup> · Leszek Chybowski<sup>10</sup> 

✉ Mariusz Ptak  
mariusz.ptak@pwr.edu.pl

Mateusz Dymek  
mateusz.dymek@pwr.edu.pl

Marek Sawicki  
sawicki.marek@pwr.edu.pl

Fábio A. O. Fernandes  
fabiofernandes@ua.pt

Maciej Wnuk  
maciej.wnuk@pwr.edu.pl

Johannes Wilhelm  
johannes.wilhelm@cfturbo.com

Monika Ratajczak  
m.ratajczak@iimb.uz.zgora.pl

Daria Witkowska  
daria.witkowska@umw.edu.pl

Artur Kwiatkowski  
artur.kwiatkowski@szpital.lgnica.pl

Błażej Poźniak  
blazej.pozniak@upwr.edu.pl

Konrad Kubicki  
konrad.kubicki@umed.wroc.pl

Marta Tikhomirov  
marta.tikhomirov@upwr.edu.pl

Adam Druszczyk  
adam.druszczyk@szpital.lgnica.pl

Leszek Chybowski  
l.chybowski@pm.szczecin.pl

<sup>1</sup> Faculty of Mechanical Engineering, Wrocław University of Science and Technology, Łukasiewicza 7/9, 50-371 Wrocław, Poland

<sup>2</sup> Centre for Mechanical Technology and Automation, Department of Mechanical Engineering, University of Aveiro, Campus de Santiago, 3810-193 Aveiro, Portugal

<sup>3</sup> CFturbo GmbH, Unterer Kreuzweg 1, 01097 Dresden, Germany

<sup>4</sup> Department of Biomedical Engineering, Institute of Material and Biomedical Engineering, Faculty of Mechanical Engineering, University of Zielona Góra, Prof. Szafrana 4, 65-516 Zielona Góra, Poland

- <sup>5</sup> Department of Forensic Medicine, Wrocław Medical University, J. Mikulicza-Radeckiego 4, 50-345 Wrocław, Poland
- <sup>6</sup> Department of Neurosurgery, Provincial Specialist Hospital in Legnica, Iwaszkiewicza 5, 59-220 Legnica, Poland
- <sup>7</sup> Department of Pharmacology and Toxicology, Faculty of Veterinary Medicine, Wrocław University of Environmental and Life Sciences, Norwida 31, 50-375 Wrocław, Poland
- <sup>8</sup> Department of Neurosurgery, Wrocław Medical University, Ludwika Pasteura 1, 50-367 Wrocław, Poland
- <sup>9</sup> Faculty of Veterinary Medicine, Department of Pharmacology and Toxicology, Wrocław University of Environmental and Life Sciences, Norwida 31, 50-375 Wrocław, Poland
- <sup>10</sup> Faculty of Marine Engineering, Maritime University of Szczecin, Willowa 2, 71-650 Szczecin, Poland